sciendo

Slovak Journal of Civil Engineering

Vol. 30, 2022, No. 1, 21 – 32
DOI: 10.2478/sjce-2022-0003

THEORETICAL CORRELATIONS BETWEEN THE CUMULATIVE ABSOLUTE VELOCITY AND PERFORMANCE POINT FOR A SEISMIC ANALYSIS OF FRAMED STRUCTURES

KAHIL Amar[1*], HANNACHI Naceur Eddine[1], HAMIZI Mohand[1] and MEBARKI Ahmed[2]

Abstract

The present paper investigates the effect of the harmfulness of a potential earthquake on structural and seismic risks. It takes into account the magnitude, epicentral distance, and pseudo depth at the hypocenter as well as the soil classification in order to generate synthetic seismic motions to be considered as signal inputs for a structural seismic analysis. The most typical typology of dwellings and buildings that are widely existing in Algeria, i.e., a reinforced concrete frame structure, is considered for the case study. The results show that the theoretical models developed in this study are able to predict the performance point (spectral displacement) according to the cumulative absolute velocity. They also show that(CAV-S_d) (S_d being the spectral displacement of the performance point defined by a pushover analysis) is slightly influenced by the value of the ultimate displacements of the structures and the soil parameters (shear velocity Vs).

Address

[1*] University Mouloud Mammeri Tizi-Ouzou, Civil Engineering Department, Faculty of Construction Engineering, B.P.17, Tizi-Ouzou, 15000, Algeria.

[2] Paris-Est University, Laboratory of Multi-Scale Modeling and Simulations, MSME UMR 8208 CNRS, 5 bd Descartes, 77454, Marne-la-Vallee, France.

* ***Corresponding author:*** Kahil Amar (amar.kahil@yahoo.com)

Key words

- Artificial motions,
- Pushover,
- Performance,
- Harmfulness of earthquake,
- Cumulative absolute velocity.

1 INTRODUCTION

Many reinforced concrete framed (RCF) structures have shown inadequate capacity during past quakes (ASCE, 2017; Korkmaz et al., 2015). For the sake of the simplified and rapid performance of seismic analyses, it seems worthwhile to investigate the correlation existing between ground displacements (indicators of harmfulness) and the performance point that defines the seismic capacity of RCF.

The harmfulness of a potential earthquake ultimately depends on the intensity of the ground motion. This may concern the peak values of any displacement, velocity or acceleration, the spectral response, or integral parameters such as the Arias intensity (Arias, 1970; Fabio et al., 2021). It corresponds to the ground duration time (Dashti et al., 2010) and the cumulative absolute velocity (CAV), (EPRI,1988).

The correlation between the seismic ground motions and structural damage has been widely investigated in civil engineering (Noura et al., 2017). Consequently, the spectral displacement, which defines the performance point, is considered the key parameter in RCF seismic analysis and estimations of damage (Xia et al., 2014).

Furthermore, an inelastic structural response is found to be strongly correlated with the spectral acceleration of the input signals for specific periods (Shome et al., 1998). However, none of the potential harmfulness of an earthquake or ground motion intensity (GMI) can entirely be considered as being the unique and best governing parameter of a seismic signal. For instance, the CAV has effects during the entire course of the motion that cannot be caught by the peak values of the displacement, velocity or acceleration and the corresponding spectral response. Therefore, the present study will focus on the CAV, whereas RCF damages will be considered as being correctly defined by the performance point on the capacity curve (Du and Wang, 2013).

Capacity curves will be established for a set of six RCF structures with different ductilities that are assumed to be wide enough to match the most commonly existing typologies. For this purpose, artificial earthquakes will be generated by adopting the Sabetta & Pugliese method (Sabetta and Pugliese, 1996). The correlation between the performance point and the CAV will be investigated and modeled.

© 2022 The Author(s). This is an open access article licensed under the Creative Commons Attribution-NonCommercial-NoDerivs License (http://creativecommons.Org/licenses/by-nc-nd/3.0/).

2 CORRELATION BETWEEN THE CAV AND THE SPECTRAL DISPLACEMENT (SD)

2.1 Cumulative absolute velocity (CAV)

A ground motion intensity measure such as peak ground acceleration (Paul and Vacareanu, 2020) is used for describing the severity of an earthquake's ground motion. A new intensity measure called cumulative absolute velocity (CAV) was proposed (EPRI, 1991). Unlike peak ground acceleration, which only relates to the maximum acceleration of the time history, CAV is dependent on the whole duration. Fig. 1 is a diagram illustrating CAV (Min et al., 2020), and its mathematical expression is as follows:

$$CAV = \int_0^{t_f} |a(t)|\, dt \quad (1)$$

where:

$|a(t)|$ = the absolute motion acceleration [in $m.s^{-2}$]

t_f = duration of the total seismic motion [in s]

The CAV is equivalent to the global absolute momentum carried by a seismic motion. Investigating the possible correlation between the CAV and the structural seismic damage is considered to be a significant issue (Campbell and Bozorgnia, 2010).

The ground motion prediction equation (GMPE) for CAV developed in this paper is based on a multidisciplinary study that was sponsored by the Pacific Earthquake Engineering Research Center (PEER) (Douglas, 2021) to develop next generation attenuation (NGA) relationships for shallow crustal earthquakes in active tectonic regions (Kenneth et al., 2010).

For the present study, the GMPE adapted for CAV corresponds to the attenuation law developed by Sabetta and Pugliese (Sabetta and Pugliese, 1996). The relation given in Equation 2 is the most suitable one for our work for the following reasons:

- The large quantity of data used by Sabetta and Pugliese (generation of non-stationary artificial earthquakes according to an empirical method based on the regression of attenuation relations of a collection of earthquakes measured in Italy with around 95 accelerograms of 17 earthquakes of magnitudes of 4.6 to 6.8).
- The fact that it allows us to include information on the state of the soil (compact and hard soil, deep alluvial deposits, and shallow alluvial deposits).
- Using the magnitude scale (Ms), magnitudes are included in the interval [4.6 to 6.8] and up to distances of 100 km (Sabetta and Pugliese, 1996).

$$\log_{10}(y) = a + bM + c\log_{10}(R^2+h^2)^{1/2} + e_1S_1 + e_2S_2 \pm \sigma \quad (2)$$

with:

a,b,c = constant parameters, where a=0.133, b=0.328 and c = -1;

M = magnitude; R= epicentral distance [in Km]; = standard deviation;

h = pseudo depth at the hypocenter [in m]; it is obtained by a fitting process and results from various effects such as motion near the source and directivity (Joyner and Boore, 1981);

y = motion parameter (pseudo velocity ($m.s^{-1}$));

e_1, e_2 = constant parameters where $e_1 = 0.262$ and, $e_2 = 0.096$;

S_1, S_2 = coefficients of the site classification (see Tab. 1).

Tab .1 *Coefficients of the site classification*

Site classification	Shear velocity Vs (m/s)	S_1	S_2
Compact and hard soil	$Vs \geq 750$	0	0
Deep alluvial deposits	$360 \leq Vs \leq 750$	1	0
Shallow alluvial deposits	$180 \leq Vs \leq 360$	0	1

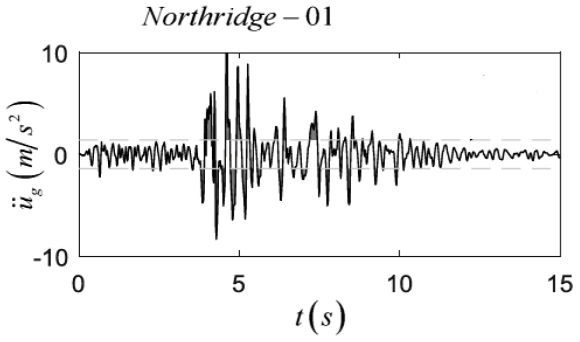
2.2 Database collection of synthetic signals

As the realization of a database of natural earthquakes is a sensitive issue, it was decided to create a database of artificial seismic signals generated by a synthetic method.

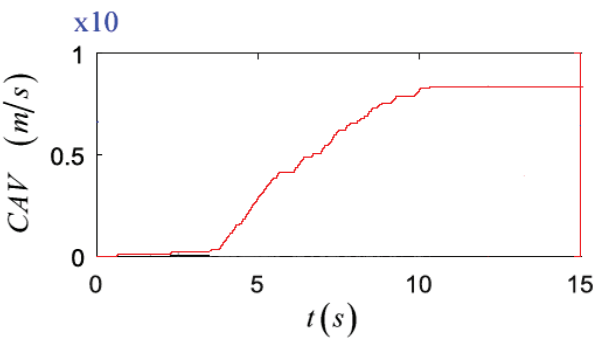
2.3 The calculation code

A code developed by Sabetta and Pugliese in 1996 was used to generate the synthetic signals. It is based on the stochastic method; its principle is to build the spectrogram of the simulated signals by analogy with the spectrograms of a natural database.

An existing code was adapted in order to generate synthetic motions, which are considered as signal inputs for structural seismic analysis. Further details about the operational procedure for this synthetic generation can be found in the technical note DEI/SARG/2005-035 (Rey and Berge, 2005).



a-Northridge-01 earthquake record



b-Cumulative absolute velocity of the Northridge- 01 earthquake record

Fig. 1 *Example of the cumulative absolute velocity of the Northridge-01 earthquake record (Anastasios and Elias, 2018).*

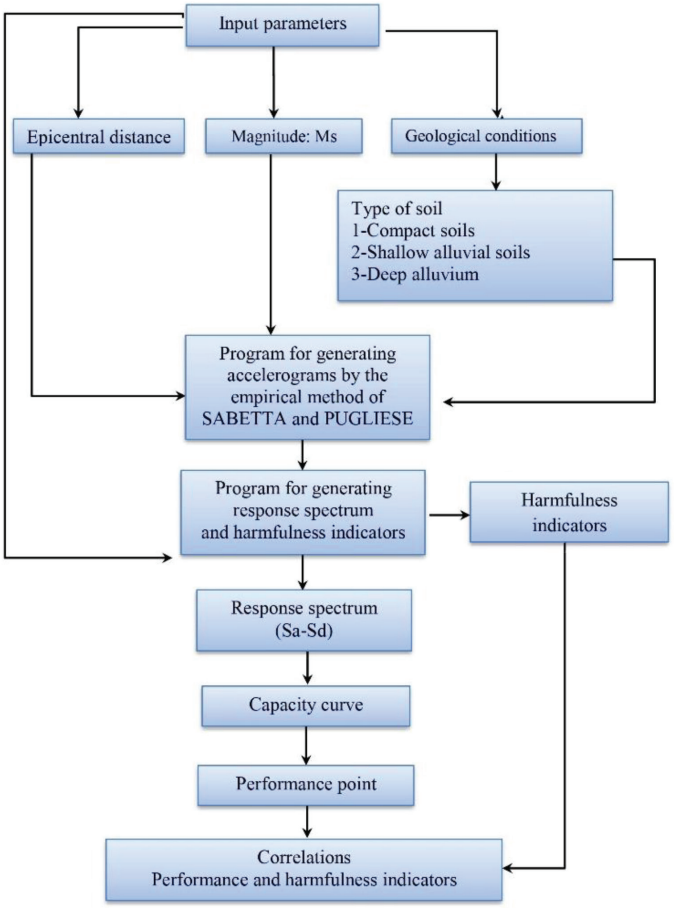


Fig. 2 *Structure of the Matlab procedure followed*

2.4 Matlab procedure

In this article, we present an overview of the Matlab procedure followed (Matlab, 2019). The difficulty in understanding this procedure is related to the fact that the numerical data are extremely numerous and that some classification logic must therefore be kept in mind (Fig. 2).

The program gathers all the procedures and permits, with seven magnitudes for three classes of soils and an epicentral distance, which varies from 0 to 100 Km with a step of 05 Km, to obtain a database of artificial earthquakes of 693 accelerograms.

3 NON-LINEAR STATIC ANALYSIS (PUSHOVER)

A static analysis conducted by progressive monotonic loading (Pushover) has been adopted in order to study the structural response (Melina et al., 2015), i.e., the top lateral displacement according to the shear effort at structure's base (ATC 40, 1996; Chopra and Goel, 1999), whereas the constitutive materials are considered as having non-linear behavior (Lenza et al., 2017).

The static pushover procedure has been widely presented, developed, and investigated over the past forty years (Saiidi and Sozen, 1981; Fajfar, 1999).

This method is also described and recommended as a tool for design and assessment purposes by the U.S. National Earthquake Hazard Reduction Program (NEHRP) (FEMA 273,1997) guidelines, and ASCE 7-16 (ASCE, 2017) for the seismic rehabilitation of existing buildings.

Moreover, the technique is accepted by the Structural Engineer's Association of California (SEAOC) (Rey and Berge, 2005), among other analytic procedures with various levels of complexity.

This procedure has been selected for its applicability to performance-based seismic design approaches, as it can be used at different design levels to verify the performance targets.

Plastic mechanisms and hinges (Fig. 3), as well as plastic adaptation and local damage, can be considered as described in the FEMA 273 guidance document (FEMA 273,1997) and the ACI 318-95 standard (ACI, 1995).

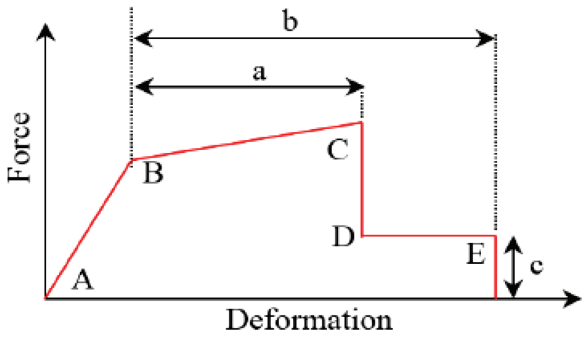
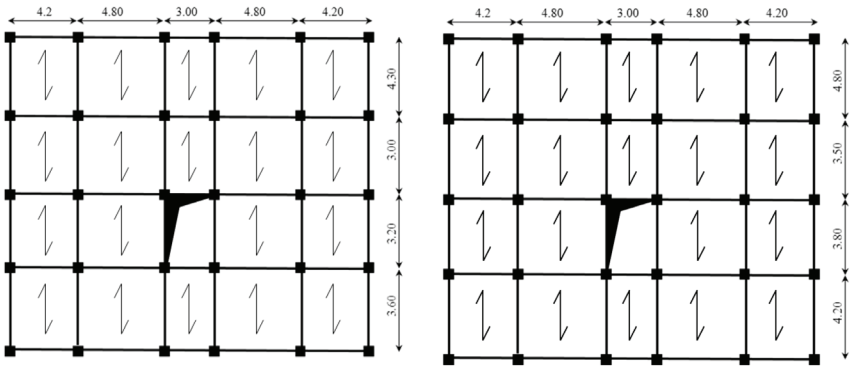


Fig. 3 *Idealized non-linear behavior of beams and columns (FEMA 273, 1997).*

The idealized bi-linear structural behavior described in Fig. 3 starts with the elastic part (branch AB) followed by the branch "BC", the slope values of which typically range within the interval



a- Structural models b- Structural models

Fig. 4 *Horizontal layouts, structural components*

0 up to 10% of the initial elastic slope, while ignoring the effects of the gravity loads acting through the lateral displacements.

Point C expresses the maximal carrying capacity of the component, beyond which a significant degradation in strength begins. The parameters 'a' and 'b' refer to the post-yield behavior phases, whereas 'c' expresses the residual bearing capacity in the "CD" branch prior to rupture (FEMA 273,1997).

4 SELECTION OF CASES STUDIED

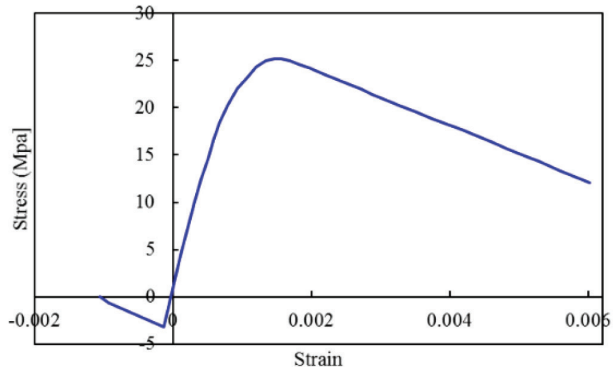
Typical typologies of some existing Algerian RCF buildings have been selected as the study cases, i.e., 6-storey model buildings (SM_i) with a 3.06 m height (a total height of 18.36 m). The horizontal layouts and cross-sections of the structural components are detailed in Fig. 4 and Tab. 2 respectively. The properties and the behavioral law of the concrete and the reinforcement of the elements are detailed in Tab. 3 and Fig. 5 respectively. They were chosen so that they cover the whole range of expected ductility and semi-ductile behavior.

Tab .2 *Cross-sections and reinforcements*

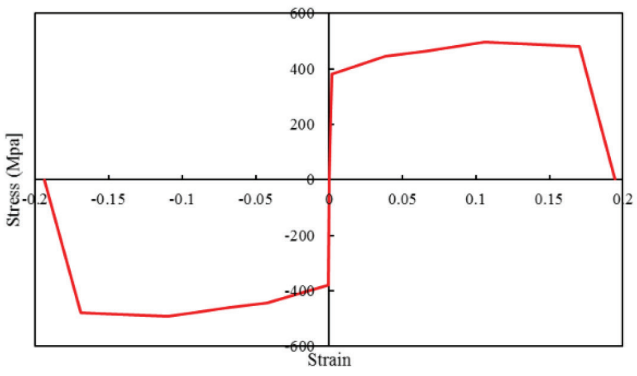
Structural models	Cross-sections (cm²)		
	Columns	Beams	
		Principal	Secondary
SM_1	30 x 30	30 x 35	25 x 30
SM_2	35 x 35	30 x 35	25 x 30
SM_3	30 x 30	25 x 30	25 x 30
SM_4	35 x 35	25 x 30	25 x 30
SM_5	30 x 30	30 x 35	25 x 30
SM_6	35 x 35	30 x 35	25 x 30
Reinforcements	8HA12 (9.05 cm²)	6HA12 (6.79 cm²)	6HA12 (6.79 cm²)

Tab .3 *Properties of the materials*

Concrete		Reinforcement	
Compression stress (MPa)	Elasticity module (MPa)	Elasticity module (MPa)	Elastic limit (MPa)
25	32164	200000	400



a-Concrete



b- Reinforcement

Fig. 5 *Stress-strain curve of the reinforcement and concrete*

4.1 Data assumed for the structures studied

The six RCF buildings studied have the same plan views. The total dead and live loads on the floor slabs are assumed to be 5.1 and 2.5 kN/m², respectively; for the roof slab, they are assumed to be 5.8 and 1.0 kN/m². The frames were designed according to reinforced concrete code BAEL 91 (BAEL, 1992) and the Algerian seismic code RPA99/version2003 (RPA99, 2003), with the following parameters: zone of high seismicity: zone III, importance class group 2, soil type S3 (soft soil), quality factor Q=1, and viscous damping ration ξ=7 %. The analysis will be performed for the zone acceleration factor A=0.25. A seismic behavior factor of R=5 was taken into consideration for RCF without any masonry infill.

4.2 Modeling approach for the inelastic analyses

The analyses were performed using the ETABS program (ETABS 18, 2019), which is a general-purpose structural analysis program for static nonlinear analyses of structures. In this study, the ETABS nonlinear version 18 has been used. A three-dimensional model of each frame structure was created to carry out the nonlinear static analyses. The beam and column elements were modeled as nonlinear frame elements with lumped plasticity by defining plastic hinges at both ends of the beams and columns, where the bilinear moment rotation relationships were assigned (ATC-72-1, 2010).

4.3 Analysis of the pushover results

The pushover analysis consisted of applying monotonically increasing, constant shape lateral load distributions to the structure under consideration. The frame model can be either 2D or 3D. The nonlinear pushover procedure in Eurocode 8 (Eurocode 8, 2003) follows the approach developed by Fajfar (Fajfar, 1999). It considers two load distributions, i.e., a uniform distribution and a modal load distribution.

The two load distributions are shown in Fig. 6. The lateral load distributions applied were increased, and the response was plotted in terms of the base shear versus the top displacement. This is the so-called pushover curve (see Fig. 6).

The pushover curve was then transformed into the response of an equivalent single degree of freedom system (SDOF) (see Fig. 7).

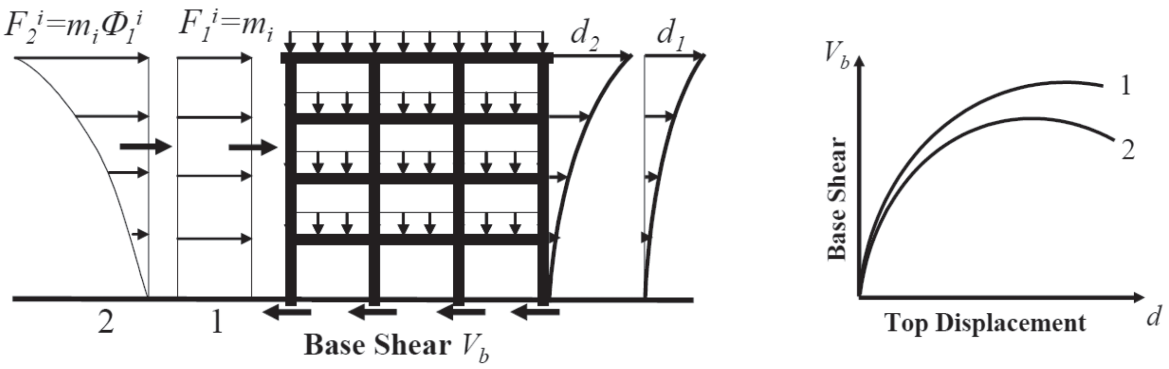


Fig. 6 *Load distributions for the pushover analysis according to Eurocode 8 and the pushover response curves*

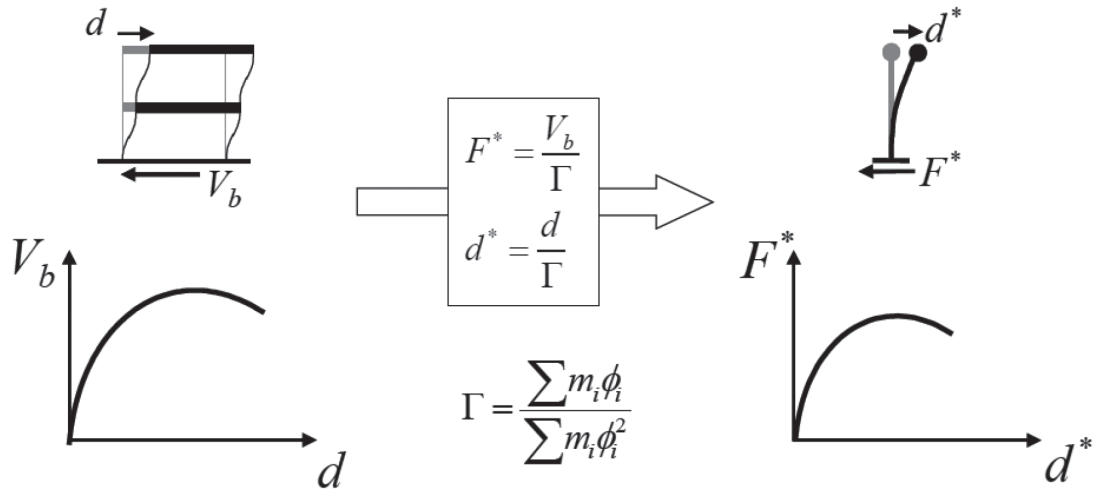


Fig. 7 *Transformation of the pushover curve into the SDOF response*

The capacity curves are classical shear force displacement representations, whereas the spectral capacity curve is derived by applying multipliers (α_1 / w) and 1/(P_{f1}.φ_{1s}) to the shear force V [in KN] and the lateral displacement δ [in m] respectively. Whereas α_1 is the mass modal coefficient, P_{f1} is the first mode participation factor, and φ_{1s} is the top amplitude (Sang et al., 2014; Fawad, 2018).

4.4 Bilinear representation of the capacity curve

The bilinear representation (Fig. 8) of the capacity curve allows us to calculate the elastic and ultimate limits in terms of the acceleration and spectral displacement for arriving at the ductility ratio μ. This defines the ratio between the ultimate lateral displacement and the yield (elastic) lateral displacement.

The equivalent bilinear curve is based on an energy equivalence criterion. For the maximum displacement value $S_{du,}$ the area under the capacity diagram must be equal to that under the bilinear curve; in other words, the areas Ω_1 and Ω_2 are equal (João and Estêvão, 2019).

In Fig. 8, S_{ay} and S_{dy} represent the spectral acceleration and spectral displacement respectively, there by corresponding to the elastic limit (Neeva and Ningthoukhongjam, 2021).

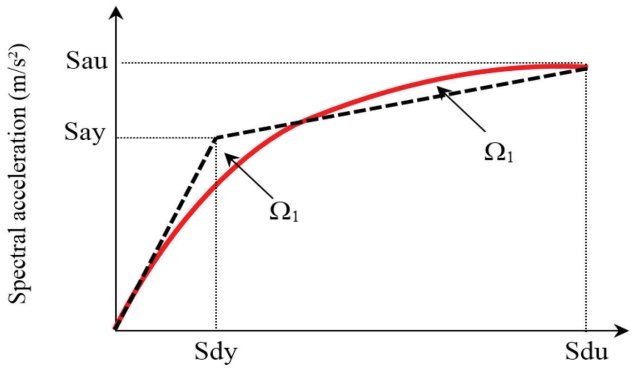


Fig. 8 *Bilinear representation of the capacity curve*

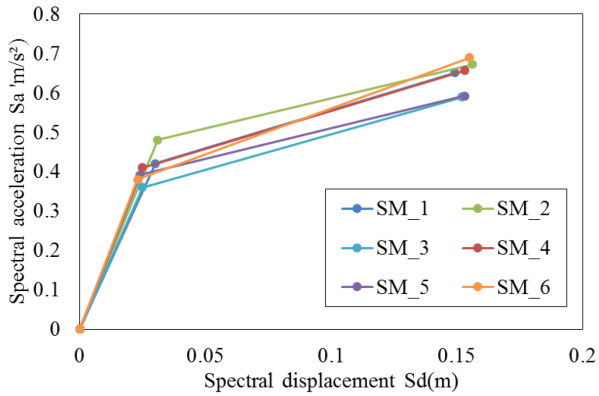


Fig. 9 *Pushover analysis results for the 6 buildings studied.*

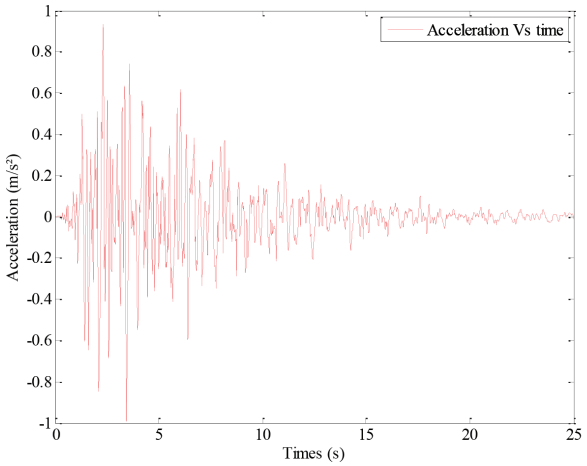


Fig. 10 *Spectral representation of the artificial demand curve.*

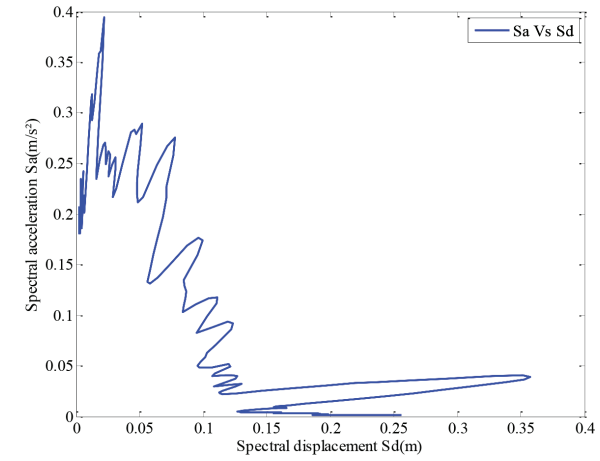
The pushover analysis was applied to the structures adopted as study cases (Tab. 4 and Fig. 9), as described above. The ductility factors obtained (Giuseppe et al.,2004; Chikh et al., 2017) are summarized in Tab. 4.

Tab. 4 *Pushover analysis and ductility results for the 6 buildings studied*

Structural models	S_d (m)	S_a (m/s²)	$\mu = \frac{S_{dy}}{S_{du}}$
SM_1	0	0	4.97
	0.03	0.42	
	0.149	0.65	
SM_2	0	0	5.03
	0.031	0.48	
	0.156	0.672	
SM_3	0	0	6.08
	0.025	0.36	
	0.152	0.589	
SM_4	0	0	6.12
	0.025	0.41	
	0.153	0.656	
SM_5	0	0	6.38
	0.024	0.392	
	0.153	0.592	
SM_6	0	0	6.74
	0.023	0.38	
	0.155	0.689	

5 PERFORMANCE POINT

The capacity spectrum method, which is widely adopted and known as acceleration, displacement, and response spectra (ADRS), was used to identify the performance point (Golafshar et al., 2020; Amin et al., 2020). It requires that both the demand curve and capacity curve have spectral representations, see Figs. 10 and 11.



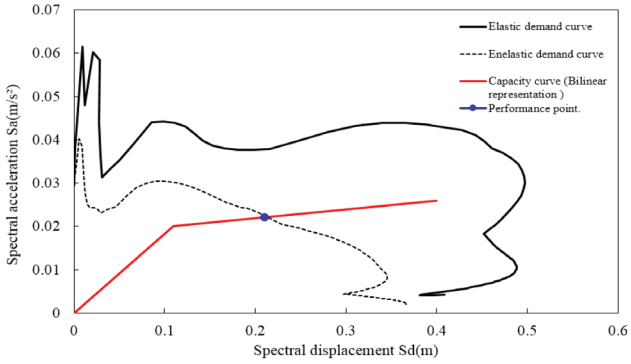


Fig. 11 *Determination of the performance point.*

The seismic demand curve (Fig. 10) was established with a linear elastic response spectrum (Tiziana et al., 2016; Amin et al., 2020). This spectrum was then transformed into an inelastic demand curve, i.e., the so-called reduced spectrum by adopting a damping ratio assumed to be equal to 5% (FEMA 440, 2004). The intersection between the capacity and the demand spectra (Fig. 11) defines the performance point.

6 EFFECT OF THE CUMULATIVE ABSOLUTE VELOCITY (CAV) ON THE PERFORMANCE POINT

The effects of the CAV on the performance point for various soil categories ($180 \leq V_S \leq 360$, $360 \leq VS \leq 750$ and $Vs \geq 750$ m / s (where Vs is the wave velocity, see Tab. 1); was investigated (Fig. 15).

The correlation between the CAV and the spectral displacement S_d is slightly influenced by the ultimate spectral displacement value (S_{du}). However, it is also greatly affected by the soil parameters (see Fig. 15).

The scattering (variability) actually depends on the wave velocity Vs: the larger the velocity, the lower the scattering.

It is therefore challenging to develop a theoretical relationship between the CAV and the spectral displacement at the design point. The results obtained show that the point cloud obtained was approximated by two functions: the first describes the ascending branch, which is similar to the power function, and the second branch is described by a linear function (an asymptote).

6.1 A theoretical relationship between CAV and S_d at the performance point

According to the results observed (Fig. 15), the most adequate relationship seems to be of the general form (see Fig. 12) at its ascending branch, where X is the decimal logarithm of CAV and whereas Y is the spectral displacement at the performance point, 'a' and 'b' being the fitting parameters (Figs. 13 and 14).

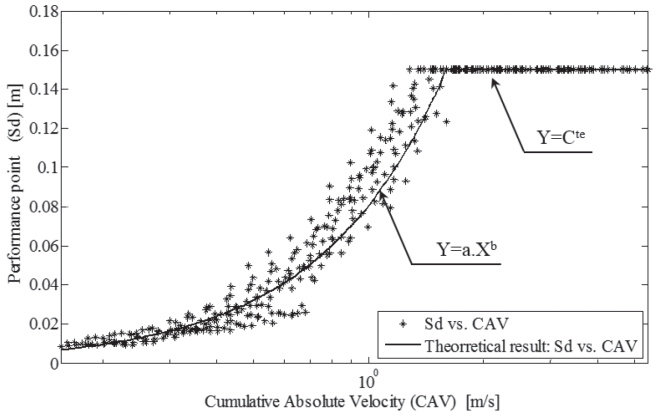


Fig. 12 *General relation between the performance point (spectral displacement) and the CAV.*

6.2 Theoretical (fitted) model and correlation between CAV and S_d

The optimal fitting corresponds to the parameters obtained by:

$$b = \frac{\overline{Ln(S_d).Ln(CAV)} - \overline{Ln(S_d)}.\overline{Ln(CAV)}}{\overline{(Ln(S_d))^2} - \overline{(Ln(S_d))}^2} \quad (3)$$

$$a = e^{\overline{(Ln(CAV)} - b.\overline{Ln(S_d)}} \quad (4)$$

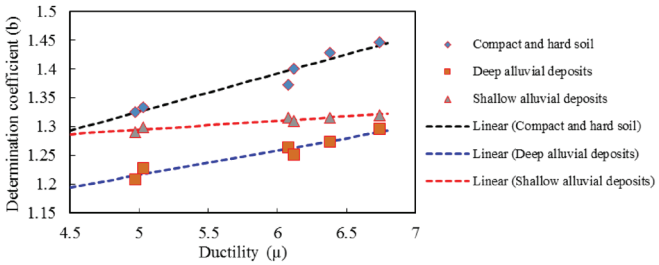
The corresponding linear correlation coefficient between CAV and S_d then becomes:

$$R = \frac{\overline{(Ln(S_d).Ln(CAV)} - \overline{Ln(S_d)}.\overline{Ln(CAV)}}{\sqrt{\left[\overline{Ln(S_d)^2} - \overline{(Ln(S_d))}^2\right].\left[\overline{(Ln(CAV)^2} - \overline{(Ln(CAV))}^2\right]}} \quad (5)$$

In equations 3,4, and 5, 'Ln' is the niparian logarithm.

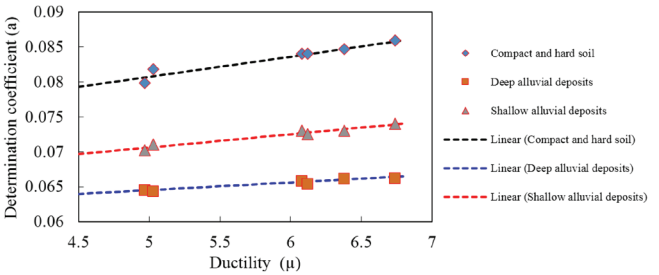
6.3 Theoretical models to predict the spectral displacement S_d at the performance point vs. CAV

The best fitted theoretical models that predict the spectral displacement S_d at the performance point according to the ductility and the CAV, as well as the threshold CAV_{se}, are summarized in Tabs. 5 to 7, where CAV_{se} is the transition point of the ascending branch and the line defined by the ultimate displacement of the structure.



Soil category	Best fitted relationship	Correlation coefficient 'R'
Compact and hard soil	S_d=0.0029 $\log_{10}$(CAV)+0.066	0.96
Shallow alluvial deposits	S_d=0.0426 $\log_{10}$ (CAV)+1.0028	0.96
Deep alluvial deposits	S_d=0.0154 $\log_{10}$ (CAV)+1.2174	0.96

Fig. 13 *Effect of the soil category on the fitting parameters (b coefficient).*



Soil category	Best fitted relationship	Correlation coefficient 'R'
Compact and hard soil	S_d=0.0029 $\log_{10}$(CAV)+0.066	0.96
Shallow alluvial deposits	S_d=0.0011 $\log_{10}$(CAV)+0.059	0.97
Deep alluvial deposits	S_d=0.0019 $\log_{10}$(CAV)+0.061	0.97

Fig. 14 *Effect of the soil category on the fitting parameters (a coefficient).*

6.4 Fitted models and results observed: S_d vs. CAV

The fitted theoretical models ''Spectral displacement S_d at the performance point''vs. "CAV" in Fig. 15 show that these (CAV-S_d) are highly correlated with coefficient R ranging from:

- 0.95 up to 0.96 for compact soil (Vs>750 m/s);
- 0.92 up to 0.98 for shallow and deep alluvial deposits.

Tab .5 *Relationship of the spectral displacement S_d at the performance point vs. CAV: case of deep alluvial deposits*

Deep alluvial deposits ($180 \le V_s \le 360$ m/s)	Ductility (μ)	CAV_{se}
$S_d = \begin{cases} (0.0019\mu + 0.0061)CAV^{(0.0154\mu+1.217)} \\ S_{du} \end{cases}$ $\begin{matrix} \text{if } CAV \le CAV_{se} \\ \text{if } CAV \ge CAV_{se} \end{matrix}\Big\}$	4.97	1.888
	5.03	1.971
	6.08	1.926
	6.12	1.971
	6.38	1.926
	6.74	1.971

Tab .6 *Relationship of the spectral displacement S_d at the performance point vs. CAV: case of shallow alluvial deposits*

Deep alluvial deposits ($180 \le V_s \le 750$ m/s)	Ductility (μ)	CAV_{se}
$S_d = \begin{cases} (0.0019\mu + 0.0061)CAV^{(0.0154\mu+1.217)} \\ S_{du} \end{cases}$ $\begin{matrix} \text{if } CAV \le CAV_{se} \\ \text{if } CAV \ge CAV_{se} \end{matrix}\Big\}$	4.97	2.0482
	5.3	2.0482
	6.8	2.0482
	6.12	2.0482
	6.38	2.0482
	6.74	2.0482

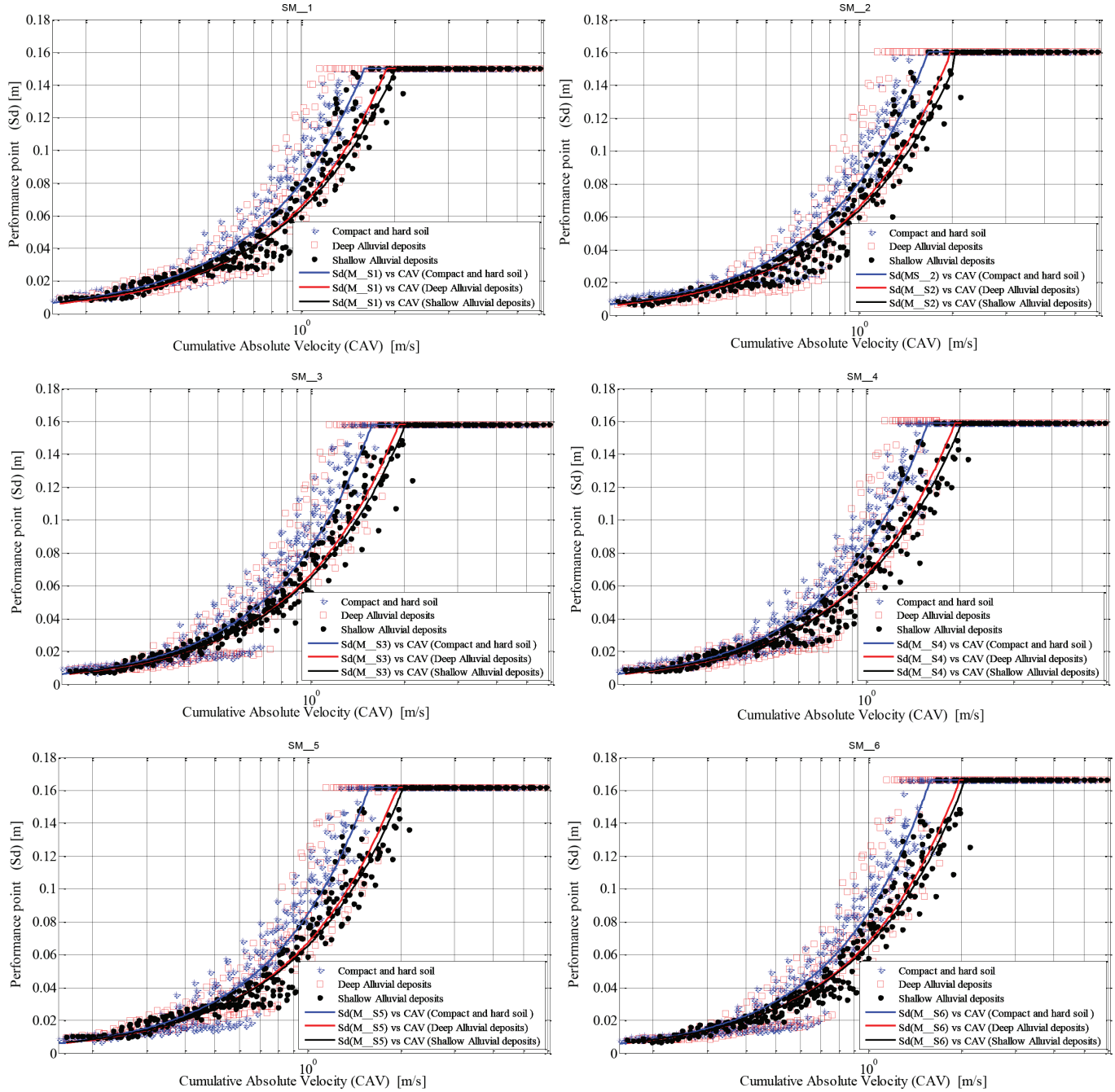


Fig. 15 *Theoretical and observed results: S_d vs. CAV.*

Tab .7 *Relationship of the spectral displacement S_d at the performance point vs. CAV: Case of compact and hard soil*

Compact and hard soil ($V_s \leq 750$ m/s)	Ductility (μ)	CAV_{sc}
$S_d = \begin{cases} (0.0029\mu+0.0662)CAV^{(0.0661\mu+0.9953)} \\ S_{du} \end{cases}$ if $CAV \leq CAV_{sc}$ if $CAV \geq CAV_{sc}$	4.97	1.599
	5.03	1.682
	6.08	1.599
	6.12	1.599
	6.38	1.599
	6.74	1.599

In order to confirm the correlation coefficients R and to ensure that the residues follow a normal distribution, a residual normality test was carried out on the whole model. The residuals were calculated at the point of performance as follows (Fig. 16):

$$\varepsilon = S_{d,model} - S_{d,simulation} \quad (6)$$

The results of the variation of the residuals are shown in Fig. 16, and the maximum and minimum residuals are shown in Figs. 17 and 18.

The results presented in Tabs. 8 and 9 show that there are not too many values outside the interval [(Mean - 2σ): (Mean + 2σ)], where σ is the standard deviation (see Fig. 16), except for the

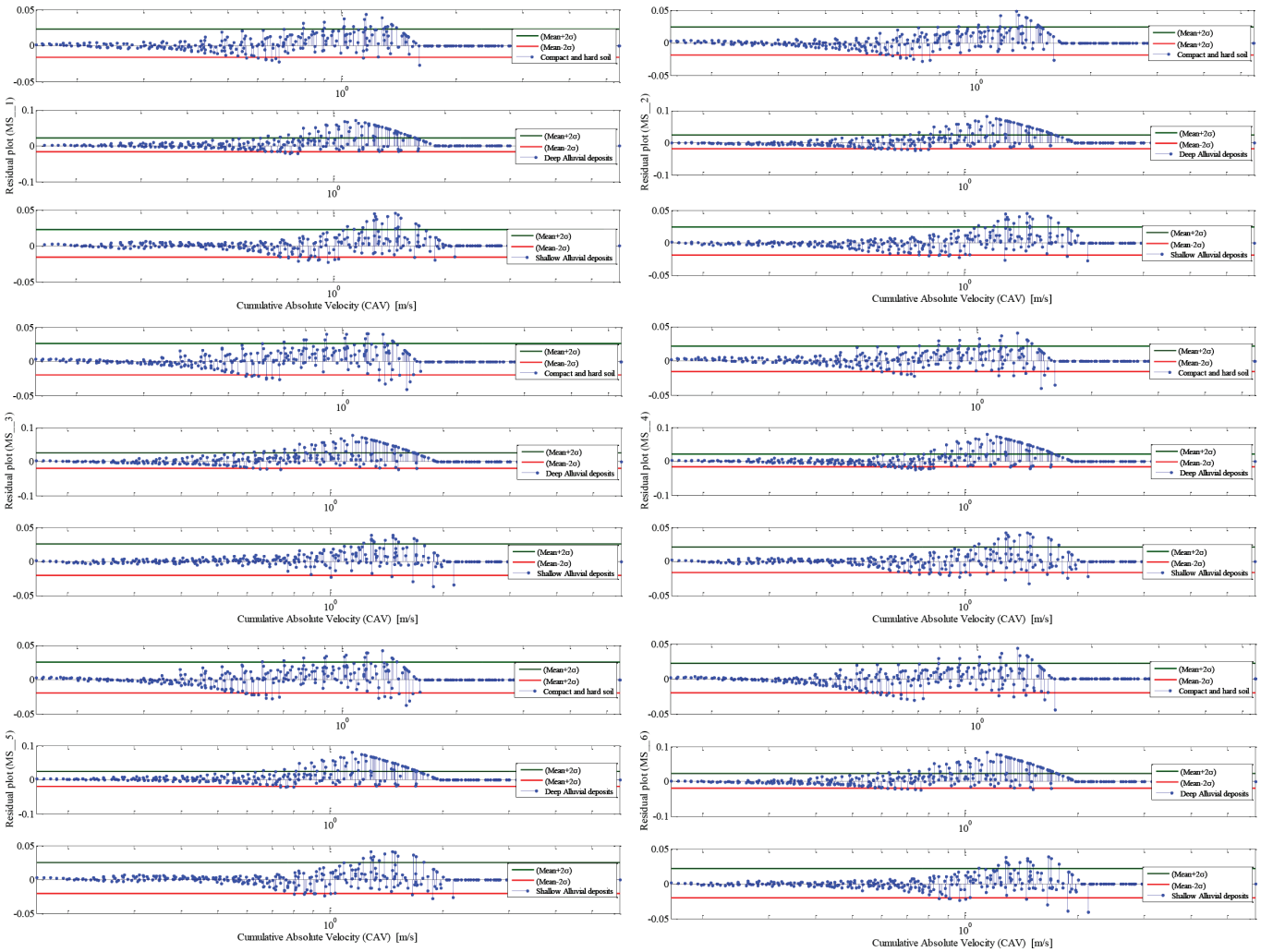


Fig. 16 *Variation of residuals at the performance point according to the CAV*

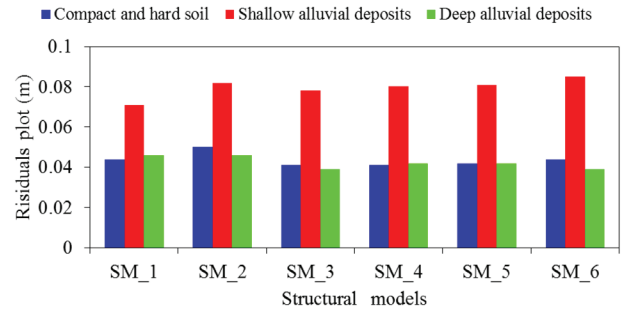


Fig. 17 *Variation of residuals at the performance point according to the CAV.*

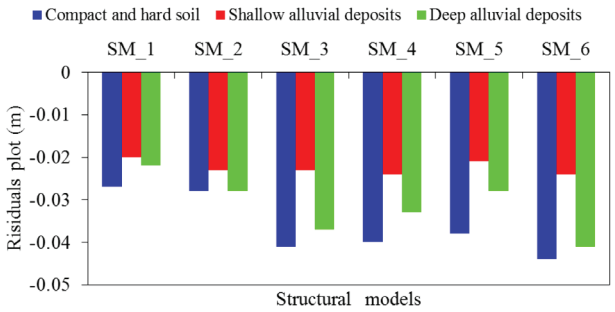


Fig. 18 *Maximum residuals at the performance point: effect of the ductility.*

SM_1 model. The difference between the mean value and the median value must be small; the observed values range from 0.01 to 0.03. It can also be noted that the distribution is symmetrical with the coefficients lying between 0.35 and 0.94, except for the SM_1. Through these test results (a normality test), it can be concluded that the proposed models are quite suitable for structural ductilities having values higher than 5.00.

7 CONCLUSION

This study has proposed a theoretical relationship between the CAV and the structural performance point (S_d). The case studies represent the existing structural typology in Algeria (reinforced concrete frame structures).

This typology of structure is taken into consideration in the present work through its ductility, which is defined by the ratio between the ultimate and elastic displacement. In order to study this typical and dominant typology in Algeria, six classes of ductility were tested numerically, and the capacity curve that reflects their behaviors was established.

In order to find a correlation between the seismic demand and the performance point, the collection of a natural earthquake database is not easy, particularly in the case of Algeria. An artificial earthquake database was created to remedy this lack based on existing mathematical models of seismic attenuation.

The results of the correlation thus obtained show the great influence of the ascending branch and the singular point for which the structural behavior reaches its asymptotic horizontal part defined by the ultimate displacement of each structural model.

The proposed models, which were obtained after adequate fitting, and the observed S_d vs. CAV results, are slightly influenced by the ultimate displacement of the structures, but are strongly influenced by the soil variability (shear velocity 'Vs') and the structural ductility. The correlation coefficient corresponding to the three categories of soils considered is between 0.92 and 0.98.

The models developed in this study allow us to obtain the point of performance of a specific structure by knowing its ductility at a given site (soil) and its shear velocity Vs. For an earthquake characterized by CAV, these models will be of great importance in a study of the large-scale vulnerability of an urban area subject to a lack of natural seismic data.

Acknowledgements

The authors are grateful to the academic institutions (University Mouloud Mammeri of Tizi-Ouzou, Algeria, and University Paris-Est, France) that partly supported the research work and the international scientific exchanges.

Tab .8 *Normality test parameters*

Structural models	Mean	Standard deviation (σ)	Mean - 2σ	Mean + 2σ	Abnormal headcount (lower)	Abnormal headcount (upper)
SM_1	0.003	0.010	-0.016	0.023	8	19
SM_2	0.002	0.011	-0.019	0.024	9	21
SM_3	0.003	0.011	-0.020	0.026	13	15
SM_4	0.002	0.009	-0.016	0.021	11	15
SM_5	0.002	0.011	-0.020	0.025	15	14
SM_6	0.001	0.011	-0.020	0.022	12	10

Tab .9 *Normality test parameters and interpretation*

Structural models	Outsized proportion	Values	Asymmetry	Flattening
SM_1	There are not too many non-standard	0.07	1.07	2.04
			The distribution is not symmetrical	The curve is pointed
SM_2		0.08	0.94	2.69
			Correct	The curve is pointed
SM_3		0.08	0.39	2.28
			Correct	The curve is pointed
SM_4		0.07	0.50	2.85
			Correct	The curve is pointed
SM_5		0.08	0.37	2.04
			Correct	The curve is pointed
SM_6		0.06	0.35	2.19
			Correct	The curve is pointed

REFERENCES

American Concrete Institute (ACI). (1995) *Building code requirements for reinforced concrete.* ACI 318-95, Mechanics and Design, 3d ed. American Concrete Institute, Detroit, MI, U.S.A.

Algerian seismic design code (RPA99/Version 2003). (2003). *National Center of Appliced Research in Earthquake Engineering,* Algeria.

Amin Saleh, A.- Amr Hussein, Z.- Gilane Abdel Hady, R. (2020) *The reliability of capacity designed components in seismic resistant systems,* International Journal of Scientific & Engineering Research, Vol 11, No 11, Nov.2020, ISSN 2229-5518.

Anastasios, I.G.- Elias, G. D. (2018) *In Quest of Optimal Intensity Measures of Rocking Behavior,*16th European Conference on Earthquake Engineering, June 2018.

Arias, A. (1970) *A measure of earthquake intensity. In Seismic Design for Nuclear Power Plants.* R. Hansen, Ed., MIT Press, Cambridge, MA, USA. pp. 438 – 483.

American Society of Civil Engineers (ASCE 7-16). (2017). *Minimum Design Loads for Buildings and Other Structures Commentary.* American Society of Civil Engineers. doi:10.1061/9780784412916.

Applied Technology Council (ATC 40). (1996). *Seismic evaluation and retrofit of concrete buildings.* ATC 40, Redwood City, CA, USA.

Applied Technology Council (ATC-72-1). (2010). *Modeling and acceptance criteria for seismic design and analysis of tall buildings.* Redwood City, CA, USA.

BAEL 91. (1992). *Règles Techniques de Conception et de Calcul des Ouvrages et Constructions en 1992,* **Béton armé suivant la méthode des é**tats limites. Edition Eyrolles.

Campbell, K.- Bozorgnia, Y. (2010) *Analysis of Cumulative Absolute Velocity (CAV) and JMA Instrumental Seismic Intensity (IJMA) Using the PEER-NGA Strong Motion Database.* PEER Report 2010/102. http://peer.berkeley.edu.

Chikh, B. - Mebarki, A. - Laouami, N. - Leblouba, M.- Mehani, Y. -Hadid, M. -Kibboua, A. - Benouar, D. (2017) *Seismic structural demands and inelastic deformation ratios: a theoretical approach.* Earthquake and Structures, 12 (4): 000-000, DOI:https://doi.org/10.12989/eas.2017.12.4.000.

Chopra, AK. - Goel, RK. (1999) *Capacity-demand-diagram methods based on inelastic design spectrum.* Earthquake Spect., 15(4):637–56.

Dashti, S. -Bray, JD. -Pestana, JM. -Riemer, M. - Wilson, D. (2010) Centrifuge *testing to evaluate and mitigate liquefaction-induced building settlement mechanisms.* Journal of geotechnical and geoenvironmental engineering, 136(7): 918–29.

Douglas, J. (2021) *Ground motion prediction equations 19642020,* http://www.gmpe.org.uk.

Du, W. - Wang, G. (2013) *A simple ground-motion prediction model for cumulative absolute velocity and model validation.* Earthquake Engineering Structural Dynamics. 42(8): 1189-1202.

Electrical Power Research Institute (EPRI). (1988). *A criterion for determining exceedance of the operating basis earthquake.* Report No. EPRI NP-5930, Palo Alto, CA, USA, 1988.

Electrical Power Research Institute (EPRI). (1991). *Standardization of Cumulative Absolute Velocity, EPRI Report RP3096- 1,* Electric Power Research Institute, Palo Alto, CA, USA,1991.

ETABS 18. (2019). *Three dimensional static and dynamic finite element analysis and design of structures V18.* Computers and Structures Inc, Berkeley, CA, USA,2019.

Eurocode 8. (2003). *Design of Structures for Earthquake Resistance,* European Committee for Standardization, 2003.

Fabio, S.-Antonio, P. - Gabriele, F.-Giovanni, L.-Lucia, L., (2021) *Simulation of non-stationary stochastic ground motions based on recent Italian earthquakes,* Bulletin of Earthquake Engineering, https://doi.org/10.1007/s10518-021-01077-1.

Fajfar, P. (1999) *Capacity spectrum method based on inelastic demand spectra.* Earthquake Engineering and Structural Dynamics. 28: 979-93.

Fawad, A. N. (2018) *Nonlinear Static Analysis Procedures for Seismic Performance Evaluation of Existing Buildings–Evolution and Issues.* Springer International Publishing AG 2018H. Rodrigues et al. (eds.). Facing the Challenges in Structural Engineering, Sustainable Civil Infrastructures, DOI 10.1007/978-3-319-61914-9_15.

Federal Emergency Management Agency (FEMA 273). (1997). *NEHRP Commentary on the Guidelines for Seismic Rehabilitation of Buildings. FEMA 273 Report, prepared by the Building Seismic Safety,* Council and the Applied Technology Council for the Federal Emergency Management Agency, Washington, D.C, USA.

Federal Emergency Management Agency (FEMA 440). (2004). *Improvement of nonlinear static seismic analysis procedures (draft) (Report ATC and FEMA).* Applied Technology Council (ATC-55 Project) and Federal Emergency Management Agency.

Giuseppe, F. - Aldo G. - Marco M. (2004) *Definition of suitable bilinear pushover curves in nonlinear static analyses,* 13th World Conference on Earthquake Engineering, Vancouver, B.C., Canada Aug. 1-6, 2004, Paper No. 1626.

Golafshar, A. - Saghafi, M. H- Eshaghi, F. (2020) A *New Method for Drawing the Capacity Spectrum for Seismic Analysis and Structural Rehabilitation,* Journal of Rehabilitation in Civil Engineering 8-3 (2020) 109-123, DOI: 10.22075/JRCE.2020.19106.1360.

João, M.- Estêvão, C. (2019). *An Integrated Computational Approach for Seismic Risk Assessment of Individual Buildings,* Applied Sciences, 2019, 9, 5088; doi:10.3390/app9235088, www.mdpi.com/journal/applsci.

Joyner, W. B. - Boore, D. M. (1981) Peak *horizontal acceleration and velocity from strong-motion records including records from the 1979 Imperial Valley, California earthquake.* Bull. Seismol. Soc. Am., 71(6): 2011–2038.

Kenneth, W. -Campbell, A.- EERI, M.- Bozorgnia, Y. (2010) A *Ground Motion Prediction Equation for the Horizontal Component of Cumulative Absolute Velocity (CAV) Based on the PEER-NGA Strong Motion Database.* Earthquake Spectra, Vol 26, No. 3, pp. 635–650, Aug. 2010; © 2010, Earthquake Engineering Research Institute.

Korkmaz, F. D.-Tugce, Y. (2015) *Earthquake Performance investigation of R/C residential buildings in Turkey.* Computers and Concrete, An Int'l Journal., 15 (6):2015.

Lenza, P., Ghersi, A., Marino, E. M., & Pellecchia, M. (2017) A *multimodal adaptive evolution of the N1 method for assessment and design of R.C. framed structures.* Earthquakes and Structures, 12(3), 271–284. https://doi.org/10.12989/EAS.2017.12.3.271.

MATLAB. (2019). Version 9.7.0.1296695 (r2019b). Natick, MA, USA. The Math Works Inc.

Melina, B- Giovanna, A.F.- Ferrara, A.- Ghersi, E.- Marino, M. – Paolo, R. P. (2015) *Seismic assessment of existing R.C. framed structures with in-plan irregularity by nonlinear static methods.* Earthquakes and Structures, An Int'l Journal., Vol. 8 No. 2, 2015.

Min,H.W.- Wangb, J.P.- Chiang, P-E.(2020) *Cumulative absolute velocity (CAV) seismic hazard assessment for Taiwan,* Journal of Earthquake Engineering, https://doi.org/10.1080/13632469.2020.1803161.

Neeva, A - Ningthoukhongjam, S. S. (2021) Development *of Fragility Curves for Different Types of RC Frame Structures.* Advances in Structural Technologies, Lecture Notes in Civil Engineering 81, https://doi.org/10.1007/978-981-15-5235-9_671.

Noura, H. - Mebarki, A. - Abed, M. (2017) *Post-quake structural damage evaluation by neural networks: theory and calibration.* European Journal of Environmental and Civil Engineering. DOI: 10.1080/19648189.2017.1304277.

Paul, O.- Vacareanu, R. (2020) *Ground Motion Model for Spectral Displacement of Intermediate-Depth Earthquakes Generated by Vrancea Seismic Source,* Geosciences 2020, 10, 282; doi:10.3390/geosciences10080282, www.mdpi.com/journal/geosciences.

Rey, J. – Berge, C. (2005) ***Étude de la variabilité de signaux synthétiques générés par trois codes de calcul et de la pertinence des indicateurs du mouvement sismique calculés sur ces signaux.*** Note technique de l'Institut Français de Radioprotection et de Sûreté Nucléaire (IRSN), DEI/SARG/2005-035.

Sabetta, F. - Pugliese, A. (1996) *Estimation of response spectra and simulation of no stationary earthquake ground motions.* Bull. Seismol. Soc. Am., 86(2):337–352.

Saiidi, M. - Sozen, M.A. (1981) *Simple Nonlinear Seismic Analysis of RC Structures.* Journal of Structural Division ASCE., 107, 937-952.

Sang, W.H.- Sung, J.H.- Hoon, K. M. - Myoungsu, S. (2014) *Improved capacity spectrum method with inelastic displacement ratio considering higher mode effects.* Earthquakes and Structures, An Int'l Journal., Vol. 7, No. 4, 2014.

Shome, N. C.- Bazzurro, P. - Carballo, JE. (1998) *Earthquakes, records, and nonlinear responses.* Earthquake Spectra, 14(3):469–500.

Tiziana, R. – Gehl, P- Stylianos, M.- Galasso, C.- Duffour, P. -Douglas, J. – Cook, O. (2016) *FRACAS: A capacity spectrum approach for seismic fragility assessment including record-to-record variability*. Engineering Structures Journal, http://dx.doi.org/10.1016/j.engstruct.2016.06.0430141-0296/Ó, 2016.

Xia, J. C- Huang, Z.J.- Yang, J. - Wu, P. (2014) Comparison *of the cumulative absolute velocity and acceleration peak value based on Wenchuan earthquake data.* Geodesy and Geodynamics. 5(3): 46–54.